A multi-scale analysis of the different interactions between defects and hydrogen: A review on the contribution of the elastic fields

G. Hachet, J. Li, A.M. Hallil, A. Metsue, A. Oudriss, J. Bouhattate, X. Feaugas

A multi-scale analysis of the different interactions between defects and hydrogen: a review on the contribution of the elastic fields

G. Hachet, J. Li, M. Hallil, A. Metsue, A. Oudriss, J. Bouhattate, X. Feaugas

LaSIE, Université de la Rochelle, CNRS-UMR 7356, F-17042 La Rochelle, France

Abstract - Hydrogen Embrittlement (HE) is one of the causes mainly evoked in premature rupture of industrial components exposed to an aggressive environment. Many studies have been conducted in order to understand the mechanisms involved during this degradation and the influence of the metallurgical states. Good knowledge of hydrogen interactions with crystal defects is a key element in the understanding of the different damage processes associated with HE in fcc materials. In this state of mind, we have undertaken a systematic study of these interactions in nickel alloys using coupled multi-scale approaches. These latter correspond to the association of atomistic calculations (EAM, DFT) with experimental tests: Electrochemical Permeation (EP), Secondary Ionization Mass Spectrometry (ToF-SIMS) analysis and Thermal Desorption Spectroscopy (TDS) in order to evaluate the hydrogen states in presence of different crystal defects. Among the major results, we focus our attention on the interaction between hydrogen and vacancies in nickel single crystals, the trapping and the segregation of hydrogen for several dislocation distributions (cells, PSB, GBs,…) and the contribution of the grain boundaries (GBs) as well as the precipitates to the hydrogen diffusion and trapping in nanocrystals, polycrystals and bi-crystals. In all the cases, we have questioned the impact of elastic fields associated with the defect to apparent solubility and diffusion of hydrogen. In the second part, we explore the potential impacts of hydrogen on elastic properties and their implication on the mechanisms of plasticity.

`

Introduction

It is now acted that the interactions of the environment with metals are strongly implied in the embrittlement of materials and alloys of the engineering structures and can lead to premature failures [1-5]. Among a large variety of processes which involves a stress/strain state and an aggressive environment, we shall note that the impact of the internal and/or external hydrogen can lead to severe loss of functional properties. A key element for the understanding of hydrogen embrittlement is based on a good knowledge of the interactions between the solute and the metallurgical state of the metal. In particular, hydrogen bonds favorably with defects and affect the physical and chemical properties of metal [6]. Through the so-called trapping phenomenon, the metallurgical state and structural defects can affect the apparent solubility and the diffusion coefficient of the solute which, sometimes, can explain why literature data on the subject exhibit some incoherence. As it has been widely established in literature, the electrochemical permeation technique and the thermal desorption spectroscopy can be used to extract and to classify the different hydrogen concentrations based on the difference in binding forces between hydrogen and the trapping sites. The lower, medium and higher binding energies correspond to the insertion in the interstitial sites C_L (0.1 to 0.2 eV), in the reversible trapping sites C_{Tr} (around 0.3 eV) associated with elastic field near edge dislocations network and/or semi-coherent precipitates the insertion in irreversible or deep trapping sites, C_{Tir} (0.5 to 0.6 eV) associated with dislocation core and/or vacancy [9,10], respectively. In each case, there is a purely mechanical contribution and a contribution of chemical origin that is not always easy to distinguish, especially at the atomic scale. In this work, we restrict our contribution to the question of the multiple interactions between a solute and the elastic stress field at the different microstructural scales and their implications on the apparent solubility and diffusivity of hydrogen. We begin our analysis by a brief presentation of the different techniques used in our work. Then the thermodynamic framework is recalled for an easy questioning of the couplings between mechanics and diffusion. Then, we give a brief reminder of the different origins of the strain fields and their gradients to finally illustrate our discussion on multiple cases recently investigated in our group.

1 – Brief review of the different techniques used

In this section, we recall briefly the different techniques used in our work to identify on the one hand the various microstructural defects studied and, on the other hand, the experimental and the numerical investigation methods that have been used to characterize the interaction of hydrogen with these defects. Dislocation and vacancy organization in nickel single crystal, bi-crystals and polycrystals have been investigated using a JEOL JEM 2011 transmission electron microscope (TEM) operating at 200 kV. Foils for transmission electron microscopy (TEM) were thinned in a double twin-jet electro-polisher using electrolytes with the conditions described previously [12]. We focus our attention on differing dislocation features issues to tensile and cyclic loading of (001) single crystal orientation, grain-boundaries with four misorientations and (001) single crystal with different hydrogen charging conditions. Dislocation densities were measured using the standard intersection method from TEM micrographs collected by Digital Micrograph™ software [11,12]. The size of vacancies cluster is obtained from classical bright field conditions. The vacancy concentrations have been evaluated using differential scanning calorimetry (DSC) as previously describe [13]. DSC measurements were performed using a Q100 TA Instruments DSC apparatus. The heating of the samples was carried out linearly from 273 to 723 K at a rate of 10 K min^{-1}. The existence of an exothermic peak in the evolution of the heat flow as a function of temperature

is associated with the annihilation of vacancies, and the area of this peak corresponds to the vacancy stored energy. The equilibrium vacancy concentration is obtained using the formation energy of a vacancy deduced from our DFT calculations and exothermic peak (1.49 to 1.52 eV between 0 K to 1200 K [14, 15]). The grain-boundary character distribution is investigated using crystallographic orientation mapping data extracted from electron backscatter diffraction (EBSD) analyses as previously proposed (EBSD was carried out using an EDAX/TSL OIM system coupled to a FEI Quanta 200 ESEMFEG scanning electron microscope) [16]. For polycrystalline structure, grain boundaries are categorized into two families: the special GBs (Σ29) corresponding mainly to the Σ^{3n} in nickel [16] (Σ3, Σ9 and Σ27), and random GBs (>Σ29). For bi-crystals, grain-boundaries with four misorientations have been identified: Σ11-50°30<110>{311}, Σ11-129°30<110>{332}, Σ3-70°30<110>{111} and Σ5-37°<100>{310} (Σx-θ <hkl>{uvw} with x the index of Coincidence Site Lattice (CSL), θ the rotation angle, <hkl> the rotation axis and {uvw} the grain boundary plane) [17,18].

To quantify the hydrogen concentration and the maximum solubility in nickel, we use Thermal Desorption Spectroscopy (TDS, Jobin Yvon Horiba EMGA-621W hydrogen analyzer) composed of an impulsion furnace system coupled with a thermal conductivity detector [9, 15,16]. The procedure consists to measure the hydrogen concentration in the pre-charged samples by fusion. The pre-charging conditions are defined in the Volmer domain of cathodic electrochemical potential range in an alkaline solution of 0.1 M NaOH at room temperature [15, 16]. According to thermodynamic and kinetic analysis the over potential range explored correspond to a fugacity of 10^5 to 4. 10^7 Pa at 300K [19]. Electrochemical Permeation (EP) is the main technique used to detect the mechanisms of diffusion and trapping of hydrogen in different microstructures in our laboratory [15, 16, 20]. This technique is composed of two cells separated by a membrane with an exposed surface in contact with an electrolytic solution. The charging side or entry side of the membrane is galvanostatically polarized at a constant cathodic charging current density (predefined according to the cathodic polarization curve and fugacity range defined previously) in 0.1 M NaOH (pH ~ 13). The detection side or exit side of the membrane was maintained at a constant anodic potential of ~630 mV/SSE in 0.1 M NaOH (pH ~ 13), and the hydrogen flux (current density) at this side is recorded to study the transport of hydrogen through the sample. A constant temperature is maintained between a range of 283 to 313K and both solutions were continuously deaerated by argon gas at 1.4 bar (see the reference [19] and [20] for more details). Using different conditions in term of temperature and cathodic charging current density/potential (equivalent to a specific fugacity), a sequence of charging followed by a sequence of desorption combines with TDS measurements at each step, allow to obtained the apparent diffusion coefficient D_{app}, the average concentration of hydrogen on the sample, the three different hydrogen concentrations namely interstitial C_L, reversible trapping C_{Tr}, irreversible or deep trapping sites, C_{Tir} and their respective energies [9,16]. In the specific case of grain-boundaries, the hydrogen concentration profile maps were obtained from time-of-flight SIMS measurements (TOF.SIMS5, ION-TOF GmbH, Germany) to elucidate the local distortion around GB impact on hydrogen segregation in polycrystalline structures [21].

The thermodynamic and elastic properties of nickel with hydrogen and/or vacancies were determined from *ab initio* calculations using the framework of the density functional theory (DFT) implemented in the Quantum ESPRESSO package [22]. Details about our calculations and convergence details can be found in our previous studies [14, 23-26]. First, we determine the H and vacancy concentrations at thermodynamic equilibrium with a H_2 gas at the temperature T and secondly the solubility and the jump rates of H in the bulk Ni lattice and in

the vicinity of a vacancy core are evaluated in relation with the lattice elastic distortion. For other defects, such as dislocations and grain boundaries, atomistic simulations based on the energy minimization method were performed using the LAMMPS code [27], to compute the structural and defect properties of nickel grain boundaries [17,18,29] and edge dislocation dipoles [30]. The EAM potential developed by Angelo *et al.* [28] for pure Ni and Ni–H systems has been used for this study. The hydrogen insertion sites that can be found in the GB region or dislocation edge dipole region were examined in terms of energy, excess volume and local stress state [17].

2 - Thermodynamic framework

The influence of the elastic stress/strain field on the chemical potential for solute is treated in the basis of a continuum approach with a thermodynamic framework [15,19, 31, 32]. According to the elastic work associated with the incorporation of the solute from the infinity to the solid, the modification of the chemical potential in an isothermal state can be expressed as :

$$\mu_H(C_H,\bar{\bar{\sigma}}) = \mu_0(C_{HO},0) + k_B T ln\left(\frac{C_H}{1-C_H}\right) - \Omega_a \sigma_{ij}\varepsilon_{ij}^S + \left[\frac{1}{2}S_{ijkl}\sigma_{ij}\sigma_{kl} + \frac{1}{2}\left(\frac{\partial S_{ijkl}}{\partial C_H}\right)\sigma_{ij}\sigma_{kl}\right]\Omega_a \quad (1)$$

with Ω_a is the atomic volume of the host matrix, μ_0 *and* C_{H0} the corresponding standard state chemical potential and the concentration, σ_{ij} the stress tensor, S_{ijkl} the compliance and ε_{ij}^s the strain tensor associated with the insertion of a solute in the crystal lattice, respectively. The first term of equation (1) is the H standard state with the absence of stress, the second one is the solute distribution entropy, the third term is the elastic strain energy associated with the insertion of a solute, and the fourth term is the mechanical energy in the system and its modification in relation with the impact of solute on the compliance tensor S_{ijkl}. In the absence of external stress, the stress state only depends on the elastic energy from the insertion of a solute in the crystal lattice (self-stress) or directly on elastic storage energy associated with the "defects" (precipitates, grain boundaries, vacancies, dislocations). Considering that the other contributions can be neglected, we can get a simplified form of the chemical potential:

$$\mu_H(C_H,\bar{\bar{\sigma}}) = \mu_0(C_{HO},0) + k_B T ln\left(\frac{C_H}{1-C_H}\right) - \Omega_a \sigma_{ij}\varepsilon_{ij}^S \quad (2)$$

Considering the problem of hydrogen incorporation into a crystal lattice is reduced to a spherical inclusion in a homogeneous medium (centrosymmetric problem) with anisotropic elastic properties, the strain induced by the incorporation of solute is expressed as $\varepsilon_{ij}^S = \frac{1}{3}\varepsilon_H\delta_{ij} = \frac{\bar{V}_H}{3\Omega_a}\delta_{ij}$. The partial volume of hydrogen $\bar{V}_H$ (m^3/at.) is a measurement of the volume variation induced by hydrogen insertion into the interstitial site. According to experimental data and DFT-based atomistic calculations, $\bar{V}_H$ for nickel is of the order of $2.1\times10^{-3} \pm 10^{-4}$ nm^3/at [24, 33, 34]. The first order impact in centrosymmetric case of the elastic field associated with defect is then reduced to:

$$\mu_H = \mu_0 + k_B T ln\left[\frac{C_H}{1-C_H}\right] + \sigma_m \bar{V}_H \quad (3)$$

with σ_m the hydrostatic stress associated with lattice strain induced by the defect.
On the other hand, the evaluation of the self-stress including the hydrostatic strain associated with a variation in the composition ΔC_H and a component resulting from stress applied by the crystal lattice on the expansion volume, allows to a chemical potential which takes the following form:

$$\mu_H(C_H) = \mu_0 + k_B T ln\left[\frac{C_H}{1-C_H}\right] - \frac{Y}{9}\bar{V}_H^2 \Delta C_H \quad (4)$$

Y is an elastic parameter equal to $-\frac{2E}{(1-\nu)}$ (E is the Young's modulus, ν is the Poisson's ratio) when considering isotropic elasticity and takes a more complex form when considering anisotropic elasticity. The latter case depends on the orientation and the components of the stiffness tensor (see the references [15,19] for more details). Consequently, the "apparent hydrostatic self-stress" can be expressed as: $\sigma_m = -\frac{Y}{9}\bar{V}_H\ \Delta C_H$. This approach can be extended to any other centrosymmetric "defects" (vacancy clusters, spherical precipitate, …) as $\Delta\mu_H = \sigma_m \bar{V}_d$ and $\sigma_m = -\frac{Y}{9}\bar{V}_d\ \Delta C_d$ with C_d and $\bar{V}_d$ are the concentration of these defects and their partial volume, respectively.
Based on continuum approach associated with equations (3) and (4), we can reconsider the set of equations which govern the diffusion and the solubility at stationary state first and secondly their impact on the apparent elastic properties (elastic properties of an equivalent homogeneous medium).

3 - Some orders of hydrostatic stress and their impact on apparent hydrogen solubility

For an open system equilibrated with an external system (hydrogen flux equal to zero) and in the Boltzmann approximation, the elastic model derived from the modification of the chemical potential of hydrogen due to the action of a hydrostatic stress allows to define the ratio of the local solubility of a solute under a hydrostatic stress field (C_H) to the solubility of the solute in a stress-free crystal (C_0) at the temperature T [14]:

$$\frac{C_H}{C_0} = exp\left[\frac{\sigma_m \bar{V}_H}{k_B\, T}\right] \quad (5)$$

At room temperature, the theoretical impact of hydrostatic stress on the apparent solubility ratio is illustrated in figure 1. An increase of one decade of hydrogen solubility can be predicted for an hydrostatic stress of 5 GPa. The self-stress contribution on the solubility ratio can be neglected because the self-stress stays lower than 5 MPa for an hydrogen content of 7 wppm (experimental related solubility at room temperature and atmospheric pressure, 4.15 x 10^{-4} H/Ni) which allows to a solubility ratio equal to 1.003. Near a basic crystalline defects, the hydrostatic stress induced is in the GPa order range : on the order of 0.5 GPa for octahedral site near a vacancy [14], 1 GPa for interstitial site close to the edge dislocation core [35] and 30 to 50 GPa for some octahedral site in a grain boundary [17, 64, 65] (refer to publications for the calculation of stresses and their location). In all these cases, these values correspond to a maximum obtained for one site and cannot be directly extended at a long-range scale without integrate the concentration of defects or solute insertion sites.

A recent work, based on DFT calculations and isotropic models [14], have questioned the implications of the elastic strain of the interstitial sites on the hydrogen solubility near vacancy in nickel. It was highlighted that a compressive hydrostatic stress acting, on the first neighboring sites except the octahedral and tetrahedral sites at a position to the center of a vacancy of respectively 0.3948 nm for octahedral site and 0.3848 nm for tetrahedral site. For both sites a local dilatation δ equal to 0.24% and 0.33% was identified and conduces to a solubility ratio equal respectively to 1.4 and 1.6. This last effect stays moderate and can partially compensate by electronic contribution ("chemical contribution") [25]. However, for a larger size centrosymmetric defects (cluster of vacancies or semi-coherent precipitates), as sources of long-range residual stress/strain, the intrinsic properties of the solid can be modified (for the diffusion and the elastic properties see the next section). Specifically, it was related recently by TEM observations that the incorporation of hydrogen in nickel single crystal induces the formation of vacancy clusters with a spherical volume of 4.2 nm^3 (with T=300 K, C_H=7 wppm and C_V=0.15 x C_H) [15, 26]. This size corresponds to a cluster of around 1000 vacancies which can induce, with the isotropic approximation, a hydrostatic stress in the order of 1.3 GPa ($\sigma_m = -\frac{Y}{9}\bar{V}_d\ \Delta C_d$) and consequently an increase of the apparent solubility by a factor of 2.5.

For the precipitates, the excess of solubility is mainly related to the elastic strain accommodation associated to strain incompatibility. This last one results to the difference between interatomic distances associated with the precipitates and the matrix, and it is a function of the degree of coherence δ of the precipitate/matrix and the volume fraction f_V of precipitate. The order of magnitude of the excess of solubility is 6 for M_xC_y carbides and 300 for TiC precipitates in martensitic steel in agreement with experimental data [20, 36]. For nickel base alloys, our recent experimental work with semi-coherent γ' precipitates in Waspaloy and Inconel 718 alloys relates an apparent solubility ratio which can be reach 3.25 and 2.36, respectively [37]. Consequently, a large hydrogen content can be stored with the addition of a semi-coherent precipitates. For the other configurations, the chemical and electrical effect (bond change) is also have contribution on ground-state energy around precipitate (short range interaction) in relation with trapping processes (see as example reference [63]).

Strain incompatibilities between some microstructural components can be also a source of residual stresses which potentially modify the local solubility of hydrogen. When considering heterogeneous distributions of dislocations, long-range internal stresses can develop and induce hydrostatic stresses with an amplitude in the order of 0.2 GPa near dislocations walls which allows to an excess of solubility ratio equal to 1.3 [30,38]. The direct relation between long-range internal stresses and the dislocation density suggests a direct proportionality between the excess of the solubility and the dislocation density. However, the experimental data relate only an increase of the apparent solubility of 8% for quenched and tempered martensitic steels [36] and 4% for a density of $2.5x10^{14}$ m^{-2} for nickel single crystal deformed in simple tension along the <100> axis [8]. This result highlights the difficulty to extend a local effect to a global measurement, i.e., the impact of the transition scales which integrates the length scale of the elastic strain (from 100 nm to 1 μm for heterogeneous distribution of dislocations). In the other part, the incompatibility of deformation between grains will also result in substantial hydrostatic stresses (in the order of 0.6 GPa [39]) which can lead to an increase of the local solubility to a factor 1.4.

An inclusion state and/or two phases microstructure can induce large stress concentrations near interfaces following a fabrication process and/or under mechanical loading. For instance,

in the case of α/β titanium alloys or duplex austeno-ferritic stainless steels, the hydrostatic pressures can reach 1.6 GPa [40,41], for a nodular cast iron is of the order of 0.8 GPa [42], for hydrides is of the order of 0.6 GPa [40, 43] and for oxides and/or sulphides of Manganese is of the order of 0.2 GPa [44]. Consequently, the solubility ratio in these different situations can be reach a maximum value around 2.3.

To conclude, all "macroscopic defects" or particular geometries (cavity, crack, reduction of section, …) will be the reason for stress concentration that can lead to hydrostatic pressures of several GPa. These hydrostatic pressures directly affect the partial molar volume of hydrogen of metals and alloys, thus providing a non-negligible elastic energy which can promote hydrogen solubility.

4 - The impact of self-stress and point defect stress on the apparent diffusion coefficient

The hydrogen flux and the apparent diffusion coefficient can be derived from chemical potential using first and second Fick's laws. According to equations (3) and (4), the hydrogen diffusion properties result to a chemical potential formalization that includes local concentration and hydrostatic stress arise to self-stress and stress induced by point defects. Based on the thermodynamics of irreversible processes, the phenomenological description of the solute diffusion is described by assuming a linear relationship between the flux and the driving forces, which are the concentration and the stress gradient in this present case. The relationship is expressed by an equation related to the gradient of the chemical potential, ∇μ [45,46]:

$$\bar{J} = -\bar{\bar{L}}.\nabla\mu \quad \text{with } \bar{\bar{L}} = \frac{\bar{\bar{D}}.C_H}{k_B T} \tag{6}$$

$\bar{\bar{D}}$ is the diffusion tensor, k_B is the Boltzmann constant and T is the temperature. The combination of equations (3) and (6), gives a relationship between the hydrogen flux and the apparent diffusion coefficient for a stress state [15,19]:

$$\bar{J} = -\bar{\bar{L}}.\nabla\mu = \bar{\bar{L}}.\frac{\partial\mu}{\partial C_H}\nabla C_H = -D\left[1 + \frac{Y(\bar{n})}{9}\bar{V}_H^2\frac{C_H}{k_B T}\right]\nabla C_H = -\bar{\bar{D}}_{app}\nabla C_H \tag{7}$$

Consequently the apparent diffusion coefficient $D_{app}(\bar{n})$ in the direction $\bar{n}$ is given as :

$$D_{app}(\bar{n}) = D[1 + \beta C_H] \qquad \text{and} \qquad \beta = \left[\frac{Y(\bar{n})\bar{V}_H^2}{9k_B T}\right] \tag{8}$$

This last equation clearly highlights an explicit effect of the solute concentration to the diffusion. Additionally, considering the elastic anisotropy, the variation of $Y(\bar{n})$ as a function of the crystallographic orientation $\bar{n}$ =[hkl], allows a direct impact on the apparent diffusion coefficient [15]. Figure 2a illustrates these both effects in the case of the hydrogen self-stress in nickel single crystal. The order of the self-stress implication stays lower than 0.1 for 35 wppm (0.025 for 7 wppm) but highlights clearly the potential implication of the hydrogen concentration and the possibility to obtain an anisotropic diffusion behavior in relation with elastic anisotropy.
Experimental data of this anisotropy was initially reported by Brass *et al.* for two crystallographic orientations (<001> and <110>) [47]. More recently, a significant effect of crystallographic orientation on hydrogen diffusivity was observed by Li *et al* for several

crystallographic orientations: ⟨100⟩, ⟨110⟩, ⟨219⟩ and ⟨111⟩ with a hydrogen concentration of 7 wppm [15]. According to the theoretical approach hydrogen diffusion is the fastest along the ⟨111⟩ orientation and the slowest along the ⟨100⟩ orientation. As reported by Li *et al.*, the experimental data, the apparent diffusion coefficients could be ranked as follows: $D_{\langle 111\rangle} > D_{\langle 110\rangle} > D_{\langle 219\rangle} > D_{\langle 100\rangle}$ for a same hydrogen content of 7 wppm [15] ($D_{<111>} = 17.5\times10^{-14}$ m²/s, $D_{<110>} = 11.2\times10^{-14}$ m²/s, $D_{<219>}= 9.3\times10^{-14}$ m²/s and $D_{<100>}= 7.1\times10^{-14}$ m²/s). The impact of crystallographic orientation on apparent diffusion coefficient is clearly higher than the one predicted by Eq. 8 ($\Delta D/D=D_{<111>}/D-1$ for the orientation <111> is equal to 4 with $D=3.5\times10^{-14}$ m²/s [25, 48, 49] instead of the modeling prediction: eq. (8) with a value around 0.02 for 7 wppm, see figure 2a). Moreover, the impact of the hydrogen content on the apparent diffusion coefficient has been experimentally questioned for the orientation <001> in nickel single crystal [15,19]. A linear relation between D_{app} and C_H is related by the authors which allows an experimental value of β equal to 0.29 instead of the one predict by the model equal to 0.01 (eq. 8 and figure 2a). The discrepancy between the model and experimental data motivates to reconsider the origin of the impact of solute content on the apparent diffusion coefficient. Based on the fact that hydrogen content promotes the formation of vacancies and vacancy clusters [15,16,26,33,50], we have recently proposed that D_{app} is affected more by the elastic stress field induced by vacancy clusters than the solute itself [15].

From a thermodynamic point of view, DFT calculations have demonstrated that hydrogen decreases the formation energy of vacancies in nickel [24,51,52]. This result is also supported by experimental data reported by Fukai *et al.* [33,50], Oudriss *et al.* [16], Li *et al.* [15] and Hachet *et al.* [26] obtained in Ni single and poly-crystals. Hydrogen incorporated into nickel matrix induces a quite linear increase in vacancy concentration ($C_{Vac}=k\times C_H$). A lower value of k for polycrystalline nickel (k=0.15) than < 001> oriented nickel single crystal (k=1) indicates a significant contribution of the grain boundary to vacancy concentration. Moreover, recent TEM observations relate the formation of vacancy clusters with an average spherical volume of 4.2 nm^3 for 7 wppm of hydrogen in nickel single crystal [26]. Following these observations, equations (2), (4) and (8) are reconsidered to take into account the elastic stress/strain fields arisen from vacancy clusters. According to Li *et al.*'s [15], the apparent diffusion coefficient is determined as a function of the number of vacancies into a cluster n_V and the partial molar volume of vacancy $\bar{V}_{Vac}$:

$$\bar{D}_{app}(\bar{n}) = D[1+\beta C_H] \qquad \text{with} \quad \beta = k\left[\frac{Y(\bar{n})(n_{Vac}\bar{V}_{Vac})^2}{9k_BT}\right] \tag{9}$$

As illustrated in figure 2b, the impact of a cluster of vacancies on D_{app} is more significant than the solute itself and reproduce our experimental data (hydrogen diffusion anisotropy and diffusion dependence on solute content) for a cluster of 40 vacancies and a partial molar volume of vacancy $\bar{V}_{Vac}$ equal to 2.25×10^{-6} m^3/mol [15,24]. If we obtain a same order for the different physical parameters for the continuum thermodynamic model and the experiment, this approach remains limited because we do not consider self-interstitial and we have assumed that elastic coefficients are constant and that solute content doesn't modify the electronic contributions to the energy of the system.

To bypass this difficulty and separate chemical and mechanical contributions, we have recently computed the components of the elasto-diffusion tensor d_{ijkl} [53] from first principles calculations of the elastic dipole tensors P_{ij} of hydrogen in the interstitial sites of perfect lattice nickel and at the saddle point along the migration path [54]. We have considered vacancies and vacancy clusters, but also the solute itself and self-interstitial, as sources of

residual strain in the solid. This last work allows to formalize the impact of stress/strain field of any centrosymmetric defects on the hydrogen diffusion.

5 - Some contributions of self-stress on the hydrogen segregation at grain-boundaries

The contribution of self-stress on hydrogen diffusion and segregation processes on non-defective lattice has been discussed in the previous sections. More recently, the question of stress/strain energy contribution on the segregation energy of hydrogen on the defective lattice is an interesting challenge [17-19,55]. The grain boundaries offer the opportunity to have a large variety of situations associated with the local distortion of lattice. Following this approach, we have studied grain boundaries differentiated by their energy and excess volume [17-19,29] to explore the diversity of GBs in nickel reported by Olsmted *et al.* [56]. Atomistic simulations based on the energy minimization method were performed using the LAMMPS code to compute the structural configurations of GBs and segregation energy of hydrogen [17-19]. Based on the fact that the insertion of an atom in lattice site creates a hydrostatic dilatation (hydrostatic strain) and a distortion of the volume (deviatoric strain), we have managed the evaluation of both at atomistic scale. The calculation of the elastic dipole tensor P_{ij} according to defect force method [17, 27, 62] and the hydrogen atomic volume V_H at the segregation site in different GBs offer the opportunity to question the impact of elastic energy associated with hydrogen insertion on adsorption energy (or insertion energy) E_H^{Ins} and segregation energy E_H^{Seg}. Thus, the atomic stress σ_{ij} and the elastic strain energy E_{el} by unit volume induced from the insertion of the hydrogen interstitial are related to the lattice-defect elastic tensor [17]:

$$\sigma_{ij} = \frac{P_{ij}}{V_H} = \sigma_m \delta_{ij} + \sigma_{ij}^d \;\; and \;\; E_{el} = E_{el}^d + E_{el}^m = \frac{1}{2B}(\sigma_m)^2 + \frac{1}{2G}(\sigma_d)^2 \qquad (10)$$

where σ_m and σ_d are respectively the hydrostatic stress and the deviatoric stress defined as Von Mises equivalent stress. B and G are the bulk and shear modulus respectively. E_{el}^m and E_{el}^d represent the dilatational and distortion energies. The insertion energy (or the adsorption energy) of a hydrogen atom in the nickel lattice E_H^{Ins} and the segregation energy relative to the octahedral site E_H^{Seg} are given by:

$$E_H^{Ins} = E_{Ni+H}^{Tot} - E_{Ni}^{Tot} - \frac{1}{2}E_{H_2} \quad \text{and} \quad E_H^{Seg} = (E_{GB+H}^{Tot} - E_{GB}^{Tot}) - (E_{Ni+H}^{Oct} - E_{Ni}^{Tot}) \qquad (11)$$

where E_{Ni+H}^{Tot} is the total energy of nickel lattice with a hydrogen atom, E_{Ni}^{Tot} is the total energy of nickel lattice without hydrogen atom and E_{H_2} is the chemical potential of the molecular hydrogen. E_{GB+H}^{Tot} is the total energy of GB with a hydrogen atom, E_{GB}^{Tot} is the total energy of GB and E_{Ni+H}^{Oct} is the total energy of the nickel lattice with a hydrogen atom at the octahedral site. E_H^{Ins} expresses the local modification of energy instead of E_H^{Seg} which relates the global evolution of the energy of the GB. The evolution of the hydrogen energy E_H^{Ins} as a function of the strain energy E_{el} from the insertion of a hydrogen atom is illustrated in figure 3a. Two distinct linear regimes are observed with a transition around a strain energy density about 2 GPa. The total strain energy is dominated by the hydrostatic stress for the first linear regime (E_H^{Ins} > -0.5 eV and V_H < 6.6 Å^3) while the other linear regime (E_H^{Ins} < -0.5 eV and V_H > 6.6 Å^3) is due to the contribution of the deviatoric stress. The hydrostatic stress is

significant for a low volume (V_H < 6.6 Å^3) such as an octahedral site in perfect fcc lattice. At these cubic form or similar sites, the deviatoric stress is low due to the small distortion. However, for high volume sites, the hydrostatic stress decreases and, at the same time, the distortion component of the stress is more significant than the hydrostatic volume change [17]. We examine now the correlation between the segregation energy E_H^{Seg} and the strain energy E_{H_2} from the insertion of a hydrogen atom (figure 3b). For the first regime defined previously (predominance of hydrostatic strain energy and low volume V_H), a linear relation is obtained which clearly highlights the impact of hydrostatic stress on segregation process in accordance with previous works [17,55]. However, for the second regime (E_{el} < 2 GPa, V_H > 6.6 Å^3), we observe some dispersion in our data. This last result illustrates a possible impact of the long range elastic contribution as it has been recently demonstrated [18,19]. Future prospects on the subject certainly will highlight the importance to distinguish the contribution of the short and from the long range strain field on solute segregation. Recently, the hydrogen concentration profile maps were obtained from TOF-SIMS measurements [21]. This work highlights for some specific grain-boundaries that a local distortion around GB impacts the hydrogen segregation and consequently supports the idea that long range strain field can be significant on this process.

6 - Self-stress and point defect stress impact on the elastic properties

The hydrogen-enhanced localized plasticity (HELP) model is the one of the most significant interpretation of slip localization in the hydrogen embrittlement context [57-59]. The model is based on the reduction of the energy barrier to dislocation motion through an elastic shielding effect induced by hydrogen or any other point defects [57,26]. According to the modification of the elastic properties of the matrix, this screening effect has been introduced into the classical results obtained with the elastic theory of dislocations on the base of a dimensionless "screening coefficient" of the pair interactions [58,59]. Despite the fact that this fundamental approach allows to partially explain some experimental observations [60], a clarification on the influence of hydrogen on the elastic properties has been only proposed recently [26]. A decrease of the Young's modulus of the <001> oriented nickel single crystal with hydrogen concentration has been reported [26]. Additionally, a linear relationship between $E_{<001>}$ and C_H is observed: $E_{<001>}(C_H)/ E_{<001>}(0)=1-A\times C_H$ with a slope A equal to 0.036 [26]. By using the equation of the chemical potential (eq. 3), the diffusion equation of hydrogen and the hypothesis of a hydrogen distribution in equilibrium with the local stress gradients, we can express the elastic strain due to the incorporation of hydrogen or centrosymmetric defect as follows [57,58, 26]:

$$\varepsilon_{ij} = S^*_{ijkl} = \left[S_{ijkl} + \frac{C_d \bar{V}_d^2}{9k_B T}\right]\sigma_{ij} \quad \text{and} \quad \frac{E^*_{<001>}}{E_{<001>}} = \frac{S_{1111}}{S^*_{1111}} = \frac{1}{1+\left[\frac{C_d V_d^2}{9k_B T}\right]E_{<001>}} \tag{12}$$

On the concentration range considered of this present work, the last equation can be reduced as :

$$\frac{E^*_{<001>}}{E_{<001>}} = 1 - \left[\frac{E_{<001>}\bar{V}_d^2}{9k_B T}\right]C_d \tag{13}$$

Considering only the potential impact of the hydrogen, the vacancies and the cluster of vacancies in the present discussion, we rewrite this equation to include the relation between

vacancies concentration and hydrogen content ($C_{Vac}=k\times C_H$) and the definition of C_d and V_d for the vacancy clusters assuming an additive contribution of monovacancies in an isotropic spherical cluster ($C_d= C_{Vac}/n_{Vac}$ and $\bar{V}_d = n_{Vac}\times\bar{V}_{Vac}$) introduced by Hachet *et al.* [26] :

$$\frac{E^*_{<001>}}{E_{<001>}} = 1 - \left[\frac{kE_{<001>}n_{Vac}\bar{V}^2_{Vac}}{9k_BT}\right]C_H \quad (14)$$

Thus, the experimental slope A can be questioned with theoretical approach for which A is equal to $\frac{E_{<001>}\bar{V}^2_H}{9k_BT}$ and $\frac{kE_{<001>}n_{Vac}\bar{V}^2_{Vac}}{9k_BT}$ for hydrogen and vacancy clusters, respectively. This analytical model has been improved in figure 4a for different situations. The slope A is respectively equal to 0.015% for the incorporation of hydrogen, 0.04% for vacancies and 0.036 for a cluster of vacancies with 100 vacancies. This last situation is in agreement with experimental observations with a slope of 0.036 (blue dot in figure 4a). Our DFT calculations support the low values obtained for hydrogen and vacancy cases [26]. The size of the vacancy clusters stays lower than the one observed by TEM [26]. Despite this fact, the prediction of the analytical model supports the idea that elastic shielding is more dependent of the superabundant vacancies than of a direct effect of the solute. The clustering of vacancies and the formation of self-interstitials in the conditions previously described are unknown and need further investigation.

Recently, we have explored the consequence of the modification of the elastic properties with the addition of hydrogen on edge dislocation dipoles of dislocations (elementary configuration of PSB) using molecular simulation within EAM potential [30,61]. This configuration is fundamental to explain the formation and equilibrium of dislocation pattern obtained under cyclic loading (dipolar walls, persistent slip band, …). We incorporate successively different hydrogen content, vacancies and cluster of vacancies in the elastic fields of each edge dislocations (in a Cottrell's atmosphere defined for a hydrostatic pressure *P* larger or equal to 10 GPa), then we evaluated the critical passing stress for different dipole configurations. In two last situations, we consider that defects do not trap hydrogen.

The contribution of hydrogen and defects on the solid solution strengthening is discussed with the Labusch's theory describing the strengthening due to concentrated, weak obstacles and diluted, strong obstacles distributions. The figure 4b relates the evolution of the increase shear stress due to hydrogen and defects. The insertion of hydrogen to create Cottrell atmosphere leads to an increase of the critical passing stress need to break an edge dislocation dipole in accordance with the Labusch's theory. In opposite, the presence of vacancies and vacancy clusters reduces the effect of the solute alone and supports a softening of process. This new result offers the opportunity to revisit the impact of hydrogen on cyclic behavior and it is nice illustration of shielding process induces by point defects [30, 61].

Conclusions et prospects

A fundamental aspect to elucidate the mechanisms of HE is based on a good knowledge of the interactions between the solute and different defects of the metal. With a review of our recent works, we highlight the importance of the elastic energy associated with the solute and the defects to explain some processes implicated on HE. The confrontation of experiment and modelling approaches at different scales offers the opportunity to clearly demonstrate a large contribution of elastic field on the hydrogen solubility, diffusion, segregation and on the modifications of the elastic properties. Moreover, we illustrate that deviatoric stress contribution cannot be neglected in some case in opposite to a common consideration in the

literature. The possible contribution of chemical component and the separation of this one to other contributions of the energy stays an interesting challenge.

References

[1] S.P. Lynch, Mechanistic and fractographic aspects of stress-corrosion cracking (SCC), in: Stress Corrosion Cracking. Elsevier, 3–89 (2011).

[2] R.D. Gangloff, B.P. Somerday (Eds.), Gaseous Hydrogen Embrittlement of Materials in Energy Technologies: Mechanisms, Modelling and Future Developments, Woodhead Publishing LtD, Cambridge (2012).

[3] I.M. Robertson, Hydrogen Embrittlement Understood, Metall. Mat. Trans. A, 46 (2015) 2323-234.

[4] M. Nagumo, Fundamentals of hydrogen embrittlement, Springer, Singapore, (2016).

[5] A.T. Paxton , A. P. Sutton and M. W. Finnis (Eds), The challenges of hydrogen and metals, 375 Issue 2098 Royal Society (2017).

[6] C. Blanc, I. Aubert (Eds), Mechanics - Microstructure - Corrosion Coupling Concepts, Experiments, Modeling and Cases, ISTE-Elsevier (2019)

[7] R. Kirchheim, « Hydrogen solubility and diffusibility in defective and amorphous metals », Progress in Mater. Sci., n° 32, p. 261-325, 1988.

[8] G.M. Pressouyre, « A Classification of Hydrogen Traps in Steel », Metall. Trans. A, n° 10A, p.1571-1573, 1979.

[9] S. Frappart, A. Oudriss, X. Feaugas, J. Creus, J. Bouhattate, F. Thélbault, L. Delattre and H. Marchebois, Scripta Materialia 65 (2011) 859–862.

[10] A. Oudriss, A. Fleurentin, G. Courlit E. Conforto, C. Berziou, C. Rébéré, S. Cohendoz, J.M. Sobrino, J. Creus, X. Feaugas, "Consequence of the diffusive hydrogen contents on tensile properties of martensitic steel during the desorption at room temperature" Mater. Sci. and Eng. A, 598, (2014) 420-428

[11] X. Feaugas, "On the origin of the tensile flow stress in the stainless steel AISI 316L at 300 K: back stress and effective stress" Acta Mater. vol. 47, p. 3617, 1999.

[12] A. Oudriss, X. Feaugas, "Length scales and scaling laws for dislocation cells developed during monotonic deformation of (001) nickel single crystal", International Journal of Plasticity, 78 (2016) 187-202.

[13] D. Guedes, A. Oudriss, S. Frappart, G. Courlit, S. Cohendoz, P. Girault, J. Creus, J. Bouhattate, A. Metsue, F. Thebault, L. Delattre, D. Koschel, X. Feaugas, "The influence of hydrostatic stress states on the hydrogen solubility in martensitic steels" Scripta Materialia, 84-85, (2014) 23-26.

[14] A. Metsue, A. Oudriss, X. Feaugas. Displacement field induced by a vacancy in nickel and some implications for the solubility of hydrogen (2014) Philosophical Magazine, 94 (34), pp. 3978-3991.

[15] J. Li, A. Oudriss, A. Metsue, J. Bouhattate, X. Feaugas. "Anisotropy of hydrogen diffusion in nickel single crystals: the effects of self-stress and hydrogen concentration on diffusion", Scientific Reports, Nature 7 (2017) 45041.

[16] A. Oudriss, J. Creus, J. Bouhattate, E. Conforto, C. Berziou, C. Savall, X. Feaugas, Grain size and grain-boundary effects on diffusion and trapping of hydrogen in pure nickel (2012) Acta Materialia, 60 (19), 6814-6828.

[17] A. Hallil, A. Metsue, A. Oudriss, J. Bouhattate, X. Feaugas, Segregation energy of the hydrogen at Ni Σ3 grain boundaries: some implications of the atomic volume and the interstitial self-stress (2018) Journal of Materials Science, 53 (7) 5356-5363.

[18] J. Li, A. Hallil, A. Oudriss, A. Metsue, J. Bouhattate, X. Feaugas, Segregation of the hydrogen at Nickel grain boundaries, in progress (2019).

[19] J. Li, The contribution of the grain boundary engineering to the problem of intergranular hydrogen embrittlement, phD La Rochelle University (2018).

[20] S. Frappart, X. Feaugas, J. Creus, F. Thebault, L. Delattre, H. Marchebois, " Study of the hydrogen diffusion and segregation into Fe-C-Mo martensitic HSLA steel using electrochemical permeation test", Journal of Physics and Chemistry of Solids, 71,10 (2010) 1467-1479.

[21] A. Oudriss, S. Le Guernic, Z. Wang, B. Osman Hoch, J. Bouhattate, E. Conforto, Z. Zhu, D.S. Li, X. Feaugas, "Meso-scale anisotropic hydrogen segregation near grain-boundaries in polycrystalline nickel characterized by EBSD/SIMS", Mater. Lett., 165 (2016) 217-222.

[22] P. Giannozzi, S. Baroni, N. Bonini, M. Calandra, R. Car, C. Cavazzoni, et al., J. Phys.: Cond. Matt. 21 (2009): 395502.

[23] A. Metsue, A. Oudriss, J. Bouhattate, X. Feaugas, "Contribution of the entropy on the thermodynamic equilibrium of vacancies in nickel" Journal of Chemical Physics, 140 (10), (2014) art. no. 104705.

[24] A. Metsue, A. Oudriss, X. Feaugas, "Hydrogen solubility and vacancy concentration in nickel single crystals at thermal equilibrium: New insights from statistical mechanics and ab initio calculations", Journal of Alloys and Compounds, 656 (2015) 555-567.
[25] A. Metsue, A. Oudriss, X. Feaugas .Trapping/detrapping kinetic rates of hydrogen around a vacancy in nickel and some consequences on the hydrogen-vacancy clusters thermodynamic equilibrium, Computational Materials Science, 151 (2018) 144-152.
[26] G. Hachet, A. Metsue, A. Oudriss, X. Feaugas. Influence of hydrogen on the elastic properties of nickel single crystal: A numerical and experimental investigation, Acta Materialia, 148 (2018) 280-288.
[27] S. J. Plimpton, Fast parallel algorithms for short-range molecular dynamics. J Comput Phys 117 (1995) 1–19. LAMMPS for large-scale atomic molecular massively parallel simulator, Sandia Nat. Lab. http://lammps.sandia.gov.
[28] J. E. Angelo, N. R. Moody, M. I. Baskes, Trapping of hydrogen to lattice defects in nickel. Model. Simul. Mater. Sci. Eng. 3(1995) 289–307.
[29] A. Hallil, A. Metsue, J. Bouhattate, X. Feaugas « Correlation between vacancy formation and Σ3 grain boundary structures in nickel from atomistic simulations » (2016) Philosophical Magazine, 96 (20), pp. 2088-2114.
[30] G. Hachet, A. Metsue, A. Oudriss, X. Feaugas. Effect of hydrogen on the mechanical response of <001> oriented nickel single crystal. Part I and II. International Journal of Plasticity, (2019) in progress.
[31] F. C. Larché, J. W. Cahn. The effect of self-stress in solids. Acta metall. 32, 1835-1845 (1982).
[32] R. Kirchheim, J. P. Hirth. Stress and solubility for solutes with asymmetrical distortion fields. Acta metall. 35 (1987) 2899–2903.
[33] Y. Fukai (Ed), The metal-hydrogen system basic bulk properties (2005).
[34] R. Nazarov, T. Hickel, J Neugebauer, Ab initio study of H-vacancy interactions in fcc metals: Implication for the formation of superabundant vacancies, Phys. Rev. B, n° 89 (2014) 144108-1-18.
[35] M. Lazar. Non-singular dislocation continuum theories: strain gradient elasticity vs. Peierls–Nabarro model, Philosophical Magazine, 97:34 (2017) 3246-3275.
[36] D. Guedes, A. Oudriss, J. Creus, J., Bouhattate, F. Thebault, X., Feaugas, Local approach of plasticity and hydrogen embrittlement in martensitic steel : on the impact of hydrogen flux , in BP Somerday et P. Sofronis (Eds.), Proceedings of the International Hydrogen Conference, Jackson, WY, Etats-Unis, sept. (2016).
[37] A. Oudriss, R. Milet, C. Berziou, F. Pettinari-Sturmel, M. Risbet, A. Metsue, X. Feaugas, Hydrogen solubility and trapping processes in nickel-based alloys: on the contribution of the elastic fields around γ' precipitates. Scripta mater. in progress (2019).
[38] M. Sahal, J. Creus, R. Sabot., X. Feaugas, The effects of dislocations patterns on the dissolution process of polycrystalline nickel » Acta Mater., 54 (2006) 2157-2167.
[39] D. Ilin., N. Saintier, J.M. Olive, R. Abgrall, I. Aubert. Simulation of hydrogen diffusion affected by stress-strain heterogeneity in polycrystalline stainless steel. Int. J of Hydrogen Energy, 39 (2014) 2418-2422.
[40] A.L. Helbert, X. Feaugas, I. Guillot, M. Clavel « Damage mechanisms in commercialy a-titanium alloys without (Ti-40) and with (Ti-40H) Hydrides », Metallurgical and Materials Transactions A: Physical Metallurgy and Materials Science, 29A, p. 1615-1628, 1998.
[41] V. Vignal, N. Mary, R. Oltra, J. Peultier. A mechanical-electrochemical approach for the determination of precursor sites for pitting corrosion at the microscale » Journal of the Electrochemical Society, 153 (2006) B352-B357.
[42] C. Guillemer-Neel, X. Feaugas, M. Clavel, Mechanical behaviour and damage kinetics in nodular cast iron: Damage mechanisms versus microstructural heterogeneities » Part. I, Met Trans. A, 31A, p. 3063- 3074, 2000
[43] E. Conforto, I. Guillot, X. Feaugas, Solute hydrogen and hydride phase implications on the plasticity of zirconium and titanium alloys: A review and some recent advances, Phil. Trans. of the Royal Society, A375 (2017) 2098.
[44] R. Oltra, V. Vignal, Recent advances in local probe techniques in corrosion research – analysis of the role of stress on pitting sensitivity » Corrosion Science, 49 p. 158–165, 2007.
[45] H. Kreuser, Non-equilibrium thermodynamics and its statistical foundations, Clarendon Press; Oxford, (1981).
[46] H. Mehrer Diffusion in solids: Fundamentals, methods, materials, diffusion-controlled processes, springer series in solid state science 155, (2007).
[47] A.M. Brass, A. Chanfreau, Accelerated diffusion of hydrogen along grain boundaries in nickel. Acta Mater. 44, 3823–3831 (1996).
[48] E. Wimmer, W. Wolf, J. Sticht, P. Saxe, C. Geller, R. Najafabadi, and G. Young, Temperature-dependent diffusion coefficients from ab initio computations: Hydrogen in nickel. Phys. Rev. B 77, 134305 (2008).
[49] D. Di Stefano *et al.* Acta Materialia. Vol 98, 1 (2015), Pages 306–312
[50] Y. Fukai, et al. A relation between the vacancy concentration and hydrogen concentration in the Ni–H, Co–H and Pd–H systems. J. Alloys Compd. 404–406, 247–251 (2005).

[51] R. Nazarov, T. Hickel, J. Neugebauer Vacancy formation energies in fcc metals: Influence of exchange-correlation functionals and correction schemes. Phys. Rev. B. 85, 144118 (2012).
[52] R. Nazarov, T. Hickel, J Neugebauer. Ab initio study of H-vacancy interactions in fcc metals: Implications for the formation of superabundant vacancies. Phys. Rev. B. 89, 144108 (2014).
[53] P. H. Dederichs and K. Schroeder, Phys. Rev. B 17, 2524 (1978).
[54] A. Metsue, G. Hachet, A. Oudriss, X. Feaugas, Implications of self-stress and defect-induced residual strain on hydrogen anisotropic diffusion in Ni single crystal, Phys. Rev. Mat. in progress (2019).
[55] X. Zhou, D. Marchand, D. L. McDowell, T. Zhu, J. Song, Chemomechanical origin of hydrogen trapping at grain boundaries in fcc metals. Phys Rev Lett 116 (2016) 075502–075506.
[56] D.L. Olmsted, S.M. Foiles, and E.A. Holm, Survey of computed grain boundary properties in face-centered cubic metals: I. Grain boundary energy, Acta Mater. 57 (2009) 3694–3703.
[57] P. Sofronis, H. Birnbaum, Mechanics of the hydrogen/dislocation/impurity interactions-i. Increasing shear modulus, J. Mech. Phys. Solid. 43 (1995) 49-90.
[58] J. Chateau, D. Delafosse, T. Magnin, Numerical simulations of hydrogen/dislocation interactions in fcc stainless steels. Part i: hydrogen-dislocationinteractions in bulk crystals, Acta Mater. 50 (2002) 1507-1522.
[59] D. Delafosse, Hydrogen effects on the plasticity of face centred cubic (fcc) crystals, in: R.D. Gangloff, B.P. Somerday (Eds.), Gaseous Hydrogen Embrittlement of Materials in Energy Technologies: Mechanisms, Modelling and Future Developments, vol. 2, Woodhead Publishing LtD (2012) 247-285.
[60] X. Feaugas, D. Delafosse, chapt. 9 Hydrogen and Crystal Defects Interactions: Effects on Plasticity and Fracture. In Mechanics - Microstructure - Corrosion Coupling Concepts, Experiments, Modeling and Cases. Edited by C. Blanc and I. Aubert. Published by Elsevier Ltd. (2019) 199-222.
[61] G. Hachet, Multi-scale investigation of the consequences of hydrogen on the mechanical response of cyclically strained nickel single crystal, phD of La Rochelle University (2018).
[62] R. Nazarov, J. S. Majevadia, M. Patel, M. R. Wenman, D. S. Balint, J. Neugebauer, and A. P. Sutton, First-principles calculation of the elastic dipole tensor of a point defect: Application to hydrogen in α-zirconium, Phys. Rev. B 94 (2016) 241112(R).
[63] K. Kawakami and T. Matsumiya, Numerical Analysis of Hydrogen Trap State by TiC and V_4C_3 in bcc- Fe ISIJ International 52 (2012), No. 9, 1693–1697.
[64] X. Zhou, J. Song, Effect of local stress on hydrogen segregation at grain boundaries in Metals, Materials Letters 196 (2017) 123–127.
[65] N. Chen, L. Niu, Y. Zhang, X. Shu, H. Zhou, S. Jin, G. Ran, G. Lu, F. Gao, Energetics of vacancy segregation to [100] symmetric tilt grain boundaries in bcc tungsten, Scientific Reports 6 (2016) 36955.

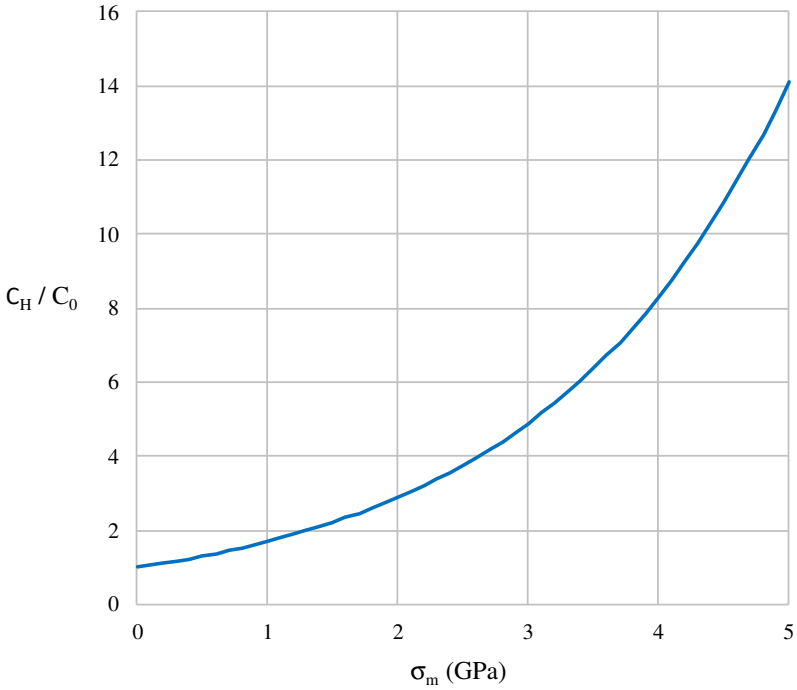

Figure 1 : Evolution of normalized hydrogen content with the hydrostatic stress at T=300K according to Eq. 5.

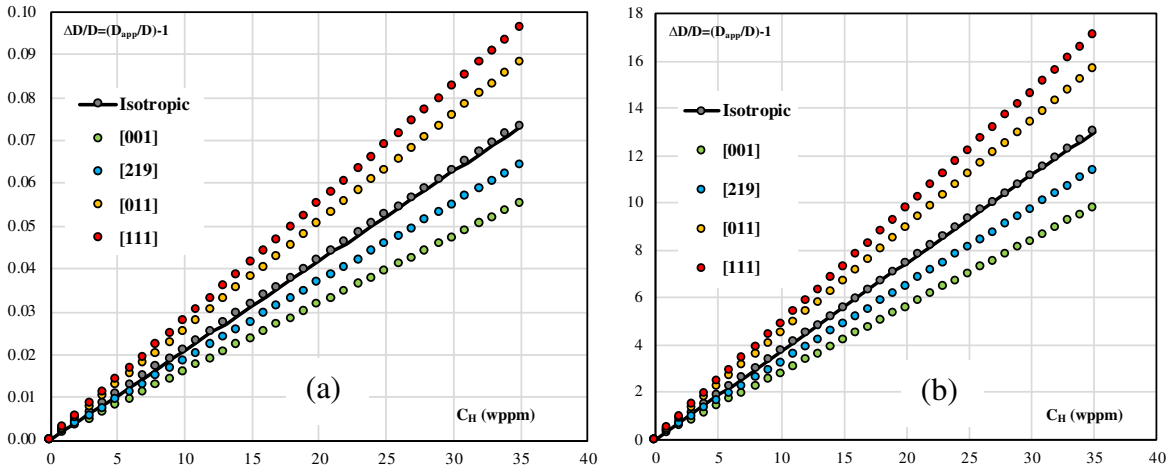

Figure 2 : Relative variation of the diffusion coefficient with the hydrogen content for different crystallographic orientations: solute impact (a) and vacancy clusters (b) [19].

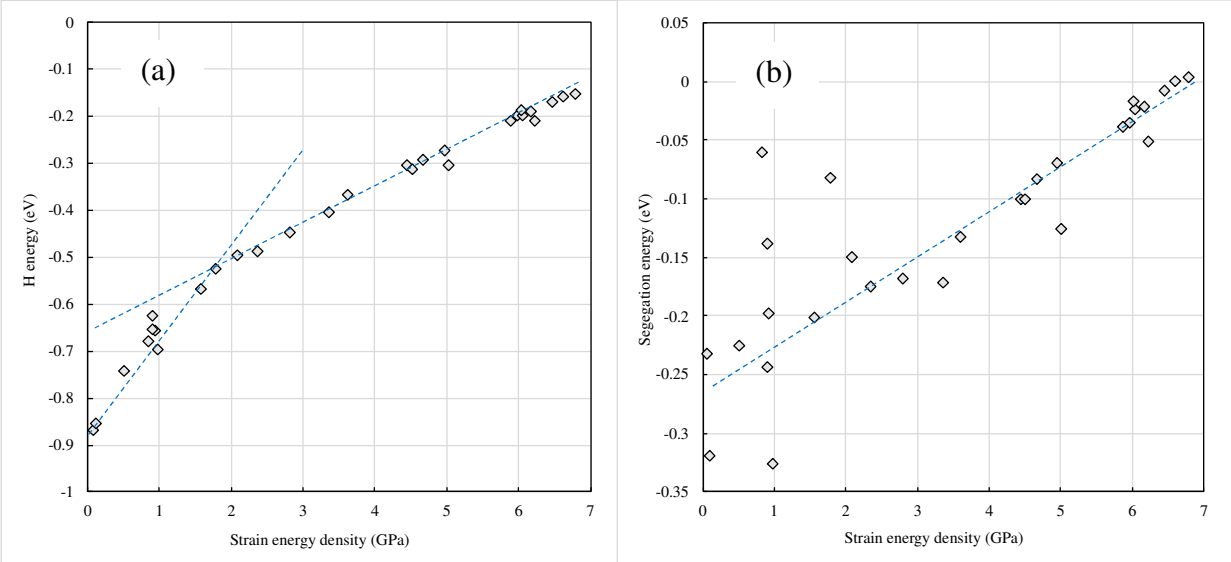

Figure 3 : Hydrogen atom energy (a) and segregation energy (b) as a function of strain energy density in the case of grain boundary in Ni [18,19].

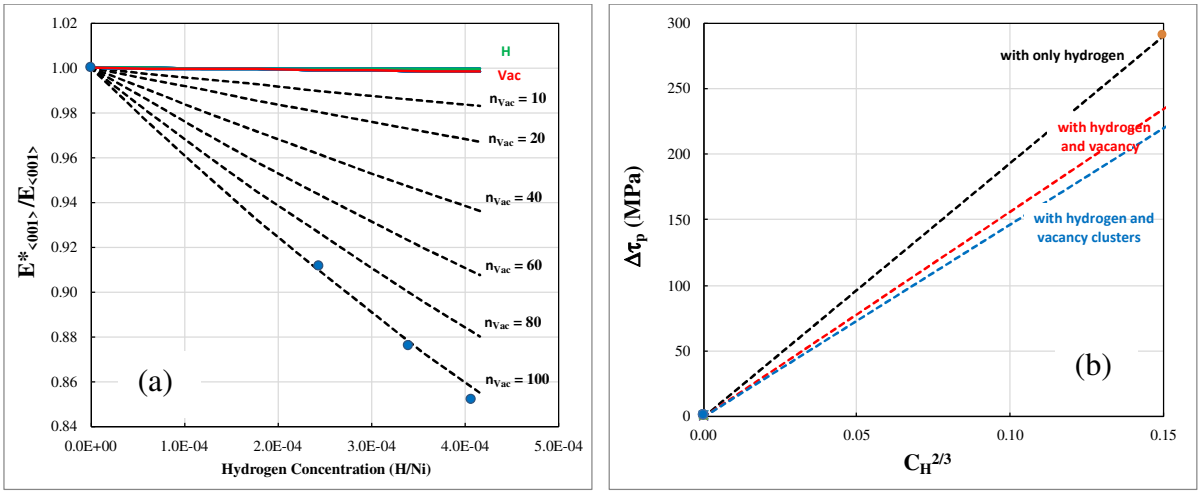

Figure 4 : Decrease of the Ni Young modulus with hydrogen content (blue dotes correspond to experimental data) (a) [26]. Increase of the shear stress due to hydrogen content without and with the addition of vacancies and vacancy clusters (b) [30,61].